

Self-similar Features in Sub-secondary Breakup of a Droplet and Ligament Mediated Fragmentation under Extreme Conditions

Saini Jatin Rao and Saptarshi Basu*

Department of Mechanical Engineering, Indian Institute of Science, Bangalore 560012, India

Droplet formation is relevant in many applications spanning natural and artificial settings. Comprehending droplet aerobreakup or air-assisted secondary atomization is challenging, especially in high-speed flow scenarios. This entails multi-scale interface deformations with intricate wave dynamics that conform to a non-linear cascade. In the present study, we look into shockwave-induced breakups and associated intermediate processes happening at smaller spatiotemporal scales across the disintegrating droplet interface at different Weber numbers ($We \sim 10^3$). We observe the undulations to follow breakup patterns that resemble a scaled-down version of a secondary atomization event. These sub-secondary breakup processes end with corrugated ligaments that generate the final daughter droplets. The size distribution of these droplets is estimated using a Depth from Defocus (DFD) technique. These illustrate the transient nature of aerobreakup, where the normalized statistics in subsequent time periods and different We are observed to follow a universal distribution. This conforms to a gamma distribution where the associated fit parameters agree well with the coefficients determined from ligament shape factors, corresponding to the limit associated with most extreme corrugations. Scaling laws based on We are deduced for the averaged statistics using a high energy chaotic breakup mechanism. These observations reinforce the idea of a self-similar mechanism for catastrophic aerobreakup of a droplet.

I. INTRODUCTION

A liquid drop undergoes rapid destabilization and fragmentation into many tiny daughter droplets when subjected to aerodynamic forcing from high-speed gas flows. This process of generating droplets or secondary atomization is relevant in many practical scenarios ranging from aerospace applications, spray coating systems, and powder production for pharmaceutical, food, or additive manufacturing applications [1]. An interactive evolution of disruptive and resistive forces establishes the breakup dynamics. The Weber number ($We = \rho_a u_a^2 d_0 / \sigma$) denotes the balance between aerodynamic and capillary forces; while Ohnesorge number ($Oh = \mu_l / \sqrt{\rho_l \sigma d_0}$) illustrates relative dominance of viscous effects over surface tension. Here d_0 is the initial droplet diameter, u_a is the free stream air velocity, σ is the surface tension, ρ is the density and μ is the viscosity where subscripts a and l represent air (gas) and liquid respectively. These dimensionless numbers are sufficient to predict various aspects of this multi-faceted problem [1–3]. The disintegrating droplet illustrates identifiable intermediate topologies, which represent different breakup modes. These modes can be delineated on a $We - Oh$ regime map. The older convention established modes like: vibrational, bag, multi-mode, stripping and catastrophic breakup [2]. However, recent advances illustrated the significant role of interfacial instabilities; hence, reclassifying the breakup modes to Rayleigh-Taylor Piercing (RTP) and Shear-Induced Entrainment (SIE) [3] as illustrated in figure 2a-b. The deforming droplet interface, where the lighter fluid (air) accelerates into the denser fluid (liquid), is destabilized through a Rayleigh-Taylor instability (RTI). This leads to RTP mode and formation of rim and bags over the deformed droplet (see figure 2a). At higher We , the aerodynamic shear on the forward facing segment of the droplet interface is significant, inducing Kelvin-Helmholtz instability (KHI) and SIE mode (see figure 2b). The KHI waves mediate the liquid transport along the periphery or a stripping process (see figure 2c). The liquid is stripped is achieved by undulation destabilization (KHI crest) in the form of sheets, ligaments and droplets as illustrated in figure 2c. This particular stripping process and the associated non-linear evolution of interface is discussed in this paper, which we will term as sub-secondary breakup processes. The KHI in the non-linear regime undergoes subsequent destabilization through other unstable mechanisms forming a wave cascade, that we will discuss below.

In a two dimensional system, when the wave crests are finite, a local wake features enables drag induced deformation and catapulting of the crest into a sheet or ligament and subsequently droplets [4, 5]. A three dimensional evolution imposes a possible transverse (or azimuthal) destabilization of the KHI wave features through other wave mechanisms including RTI. This cascading behavior is observed in primary atomization as well [6]. A temporal evolution of liquid structure length scale depicted a cascade with diminishing scales [7]. The average radius of curvature of the interface increases with time as well, indicating the formation of thin corrugated ligaments. This cascade behavior was

* Contact author: sbasu@iisc.ac.in

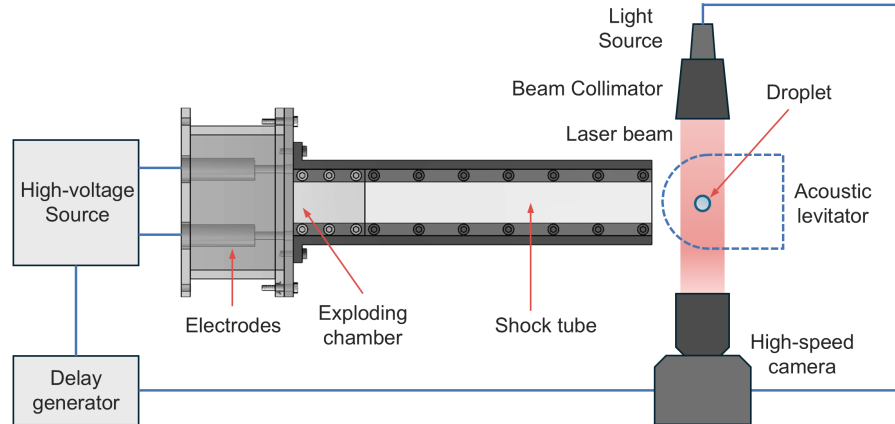


FIG. 1. Experimental setup illustrating a wire-explosion based shock tube, actuated by a pulsed high voltage source. An acoustic levitator is used to place the droplet at the opening. A shadowgraphy system is deployed for imaging.

explained using an approach based on vortex dynamics [8, 9]. A regime map for topological evolution of the local wave features was deduced based on global flow parameters. Furthermore, a recent study [10] presented the undulation breakup over the destabilized jet surface to be analogous to secondary atomization and defined a local effective We to establish a regime map accommodating different possible modes. The observed modes were morphologically similar to the droplet breakup modes at lower We .

These sub-scale processes associated with atomization events end with ligament-mediated mechanism. These ligaments play a vital role in final droplet production through the Rayleigh-Plateau instability (RPI) [11–14]. The geometric characteristic of the ligament determines the size of the distribution of the daughter droplets. Based on a model considering aggregation of possible breakup and coalescence events of the sub-elements of the ligament (imagining the corrugated ligament to be constituted of blobs matching the local diameter), a correlation was established between the shape factor and parameters associated the gamma distribution associated with the final droplet sizes [11, 15]. This can also be extended to determine parameters of a compound gamma distribution [16]. This mechanism was also extended to non-Newtonian liquids and a limit was established for these coefficients corresponding to extreme levels of corrugation.

We intend to extend these ideas to droplet aerobreakup and assess the sub-scale breakup events of the undulations or the self-similar sub-secondary atomization processes. At present, there is considerable speculation regarding the local evolution of sub-scale features, with limited studies clearly visualizing this phenomenon. These sub-scale processes illustrate a wave cascade that terminates with corrugated ligaments. In these extreme flow conditions of shock-induced atomization, we observe the ligament shape factors and the associated transient daughter droplet size distribution to correspond to extreme corrugation limit. This enables us to move towards a self-similar model for droplet disintegration in the catastrophic breakup regime. The self-similarity encompasses various aspects, including the multi-scales breakup topology and transient evolution of size distributions at aerodynamics strength, represented by We .

II. EXPERIMENTAL SETUP AND METHODS

An exploding-wire-based shock tube setup was used for the shock-droplet interaction experiments, as illustrated in figure 1. Details for the same can be found in the previous works [17–19]. However, the essential details will be briefly discussed here. A high-voltage source (2kJ pulse power, Zeonics Systech India, Z/46/12) is used to discharge electrical energy through a thin wire (35 SWG, bare copper wire) for a very short time duration ($\sim O(1)\mu s$), causing an explosion accompanied by a blast wave. This is transformed into a planar shock wave by deploying a rectangular shock tube cavity ($20mm \times 40mm \times 320mm$). An isolated DI water droplet of size $d_0 \approx 2mm$ is placed in the shock tube opening using an acoustic levitator. A digital delay generator (BNC 575) simultaneously triggers the imaging and shock tube system. The shock Mach numbers (Ma_s) are controlled by adjusting the charging voltage (V_c). Experiments are carried out at $Ma_s = 1.27, 1.39$ & 1.56 , with corresponding Weber numbers $We \approx 900, 2000$ & 4000 [20].

In the current exposition, shadow imaging is realized by using a Cavitar Cavilux smart UHS pulsed laser connected

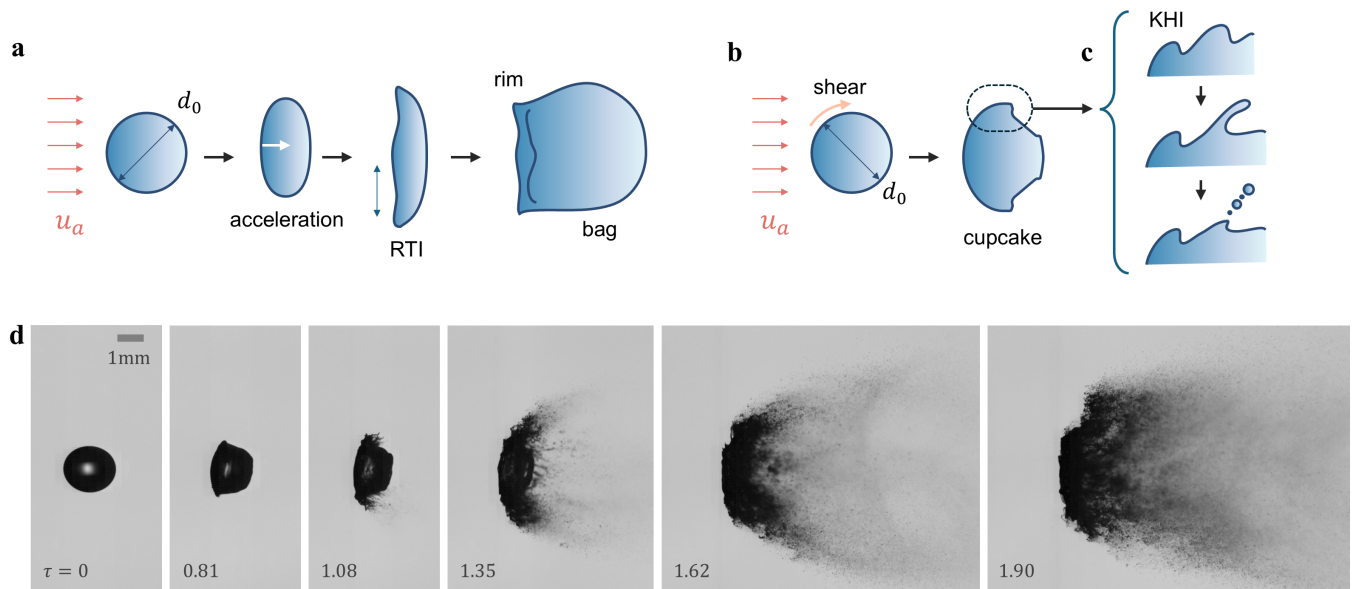


FIG. 2. Schematic illustrating (a) Rayleigh-Taylor Piercing (RTP) (b) Shear-Induced Entrainment (SIE) (c) An undulation destabilisation through sub-secondary breakup process (d) Shadow images of a shock induced breakup of a droplet at $We \approx 2000$, depicting an SIE mode.

to a beam expander and a diffuser plate for uniform background illumination. The images were captured at $75kHz$ ($93kHz$ for some instances) using a Photron SA5 camera. A $6.5\times$ Navitar zoom lens coupled with a $1.5\times$ attachment and $2\times$ objective ensured a resolution of $2.38\mu m/\text{pixel}$. A modified version of this imaging system was deployed earlier in the previous study [20] to determine the daughter droplet sizes using the Depth from Defocus (DFD) approach. An optical configuration with higher magnification, a beam splitter, and two high-speed cameras were used to acquire two simultaneous images with different extents of blurring. The sizing statistics obtained earlier are subsequently assessed here for further insights into the fragmentation process.

III. RESULTS AND DISCUSSION

A. Global overview

A global view of the shock droplet interaction at a $We \approx 2000$ is depicted in figure 2. The time stamps are clocked from the moment shockwave interacts with the droplet, and it is normalized with the inertial time scale $t_i = d_0/u_a\sqrt{\rho_a/\rho_l}$ such that $\tau = t/t_i$. In this regime, we observe SIE mode of breakup. The shock wave has minimal influence on the droplet [17], while the induced flow behind shock imposes aerodynamic disruptive forces. The drop starts deforming in the presence of non-uniform shear and pressure on the surface. It deforms to a cup-cake shape with a lip-like feature at the equator by virtue of shear and wake vortices [17]. Shear on the forward-facing segment induces liquid mass transport to the periphery, which is accompanied by unstable waves originating from KHI. This liquid is then stripped off through the other unstable wave modes, which will be discussed below (see figure 2b-c). However, to crudely describe, KHI wave crests in the non-linear regime are destabilized under the influence of local acceleration, and an azimuthal RTI enables periodic ligament formation. These ligaments then generate a fine mist of droplets through RPI, as observed in figure 2d.

B. Sub-secondary breakup processes

In aerobreakup, a globally deforming droplet interface sets up the stage for further unstable mechanisms to manifest. In the SIE breakup mode, a shear-driven KHI generates periodic perturbations to the interface (wave crests) with characteristic wavelength and growth rates. In other words, there is a characteristic spatiotemporal signature associated with these local undulations over the evolving liquid boundary. Further sub-scale evolution of these undulations

constitutes a sub-secondary breakup process.

The shear induces KHI, and the deforming droplet interface imposes acceleration-induced RTI. Both of these mechanisms create undulations over the interface. The wavelength and amplitude represent the length scale of deformation. The wavelength can be deduced using linear stability analysis, enforcing simplistic assumptions but reliable estimates [6, 17, 21]. The wavelength should be smaller than the droplet for it to manifest over the surface [17, 19]. Additionally, the growth rate of the wave amplitudes sets up a race among various modes with faster growth rates supporting early appearance. These sets a scale-based compatibility criteria. These wave crests are reminiscent of a local undulation over the interface and will be treated as a sub-scale mass of liquid body (see figure 2 and 4).

When exposed to extremely high-speed gas flows, these undulations disintegrate, resembling a portion of an independent fluid blob as illustrated in figure 3 and 4. This enables the stripping of liquid mass from the parent droplet body in a recurrent fashion [22]. The fresh surface then undergoes the next deformation cycle, setting up an undulation, again undergoing a sub-secondary breakup process.

Ligament mode: The traverse elongation of the wave crest, associated with the growth rate of the primary wave, say KHI, establishes an acceleration-induced body force. With the heavier fluid pushing rapidly into the lighter fluid, RTI generates azimuthal wave perturbations over this crest. The continued presence of transverse acceleration leads to further augmentation of these RTI wave crests, which eventually elongate with aerodynamic assistance to form ligaments. These ligaments undergo an RPI-mediated breakup into daughter droplets as illustrated in figure 3a and 4a.

However, there is another possible mechanism. The unsteady expansion of sheets is shown to be bound by unstable rims [23]. The local undulation growing transversely can also evolve into a sheet as they stretch. The presence of a rim at the leading end of this sheet-like feature is difficult to visualize from shadowgraphy images at this early stage. However, if present, the unsteady sheet expansion induces a combined RTI-RPI effect where droplets are shed through periodic ligaments from the rim [24].

Bag Mode: Another possible effect arises from the drag forces over this undulation. This undulation resembles a protrusion over the liquid surface with a bluff body-like flow around. This is similar to aerodynamic forcing over the droplet. Aerobreakup of droplets shows axisymmetric dynamics subsuming a bi-fold symmetry, dividing it into two equal halves. The undulation resembles one such half [10]. The flattening of undulation under such effects, including growth in the transverse direction, leads to the formation of sheet-like features. The drag augments the acceleration imparted over the interface in the longitudinal (gas flow) direction. This imparts RTI over this sheet in the azimuthal direction, forming bags bound by the rim. The bag grows, and the thin film ruptures, creating very fine droplets. The residual ligament fragments under the combined effect of capillary and aerodynamic forces. The rims resemble a loop, which opens up as it breaks, with the remanent base resembling independent ligaments emerging from the parent droplet body (similar to the previous case of ligament). Refer to Figures 3b-f for experimental observations and 4b for the schematic. This bag mode is similar to the RTP mode or bag breakup in secondary atomization [25].

In both of these sub-secondary processes, the RTI mechanism establishes a topology that evolves into ligaments that disintegrates through aerodynamically assisted capillary breakups. However, the ligament mode has a prominent transverse acceleration, and the bag mode illustrates the same in the longitudinal direction. The bag mode also involves an additional bag film breakup, generating very small droplets. The sheets are ruptured by the spontaneous appearance of holes bound by unstable rims. These rims shed ligaments and droplets. AS this system entail a lot of perturbations from the extreme aerodynamic forcing, multiple holes may appear, and their merges leave behind a thicker intermediate rim. This disintegrates into another class of droplets.

A higher inertia is required for this drag to manifest as waves and initiate bag mode. Hence, we observe an abundant occurrence of bag mode in this high $We - Re$ regime of present experiments, with a very rare sight of ligament mode as evident in figure 3.

There are many undulations present over the droplet interface, simultaneously fragmenting through the aforementioned sub-secondary processes. Such interactions lead to the appearance of extremely corrugated ligaments in complex groups. They sometimes appear as part of a complex web to the parent droplet segments as illustrated in figure 5. Another fascinating observation includes mushroom-shaped short ligaments or blobs resembling the remnant stamen observed in the bag-stamen breakup modes (see last row of figure 5). Transversely stretched ligaments aligned perpendicular to the gas flow are subjected to drag and deformation-induced accelerations. The RTI breakup of ligaments consists of periodic nodes that are left behind, depicting a mushroom shape as illustrated in figure 6. They are similar to nodes observed on the rim (including stamen) that appear during the bag breakup of a droplet [25, 26].

Effective local dimensionless parameters: The cascades originate for instance from each KHI wave crest of finite amplitude and terminate into daughter droplets as depicted in figure 4. An effective Weber number can be defined locally for this based on deformation scale ξ and local effective gas flow velocity u'_a as

$$We' \sim \frac{\rho_a u_a'^2 \xi}{\sigma} \quad (1)$$

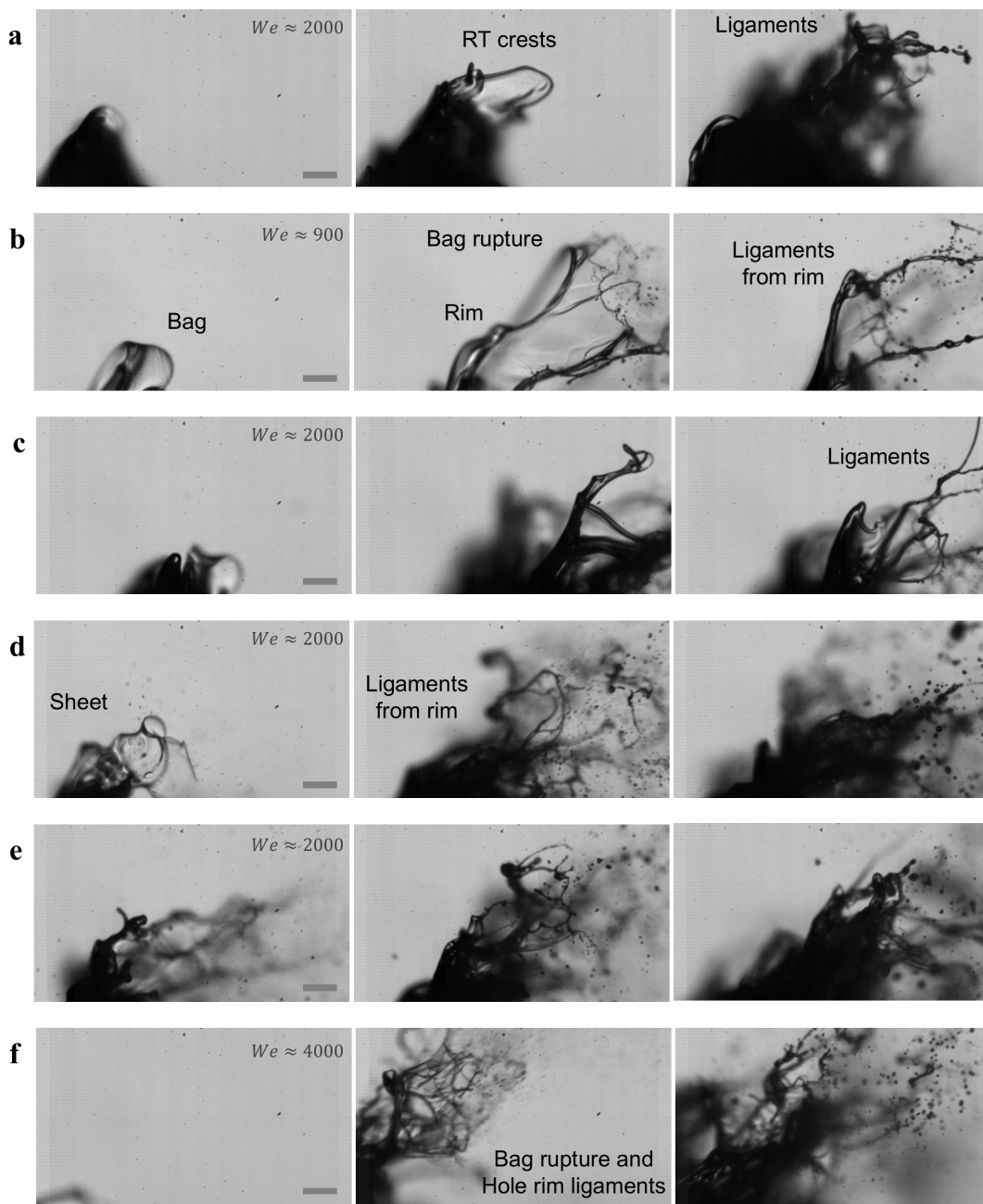


FIG. 3. Evolution of an undulation over droplet surface undergoing sub-secondary breakup processes (a) ligament mode (b-f) bag mode. The scale bar represents $100\mu m$ and consecutive frames are separated by an interval of $\Delta t = 13.33\mu s$.

A similar hypothesis bridged primary and secondary atomization events, where undulations over a destabilized liquid jet during breakup was treated as an equivalent droplet segment [10]. Based on the local effective We , the breakup dynamics were predicted for each undulation, drawing inspiration from secondary atomization. The same philosophy is extended here, and is expected to predict the modes associated with sub-secondary breakup process. Earlier studies for primary atomization [8] developed a regime map for potential modes of undulation breakup based on global dimensionless parameters. However, a local dimensionless parameter presents a self-similar approach. For viscous or non-Newtonian fluids, other relevant dimensionless numbers can be defined as well, based on these local scales. Hence We' enable predict the evolution of undulation via the ligament or bag mode discussed earlier. However determining this We' is beyond the experiment capabilities of the present study. Wang *et al.* [10] relied on the droplets generated from the undulation breakup to determine the total volume associated. Assuming undulation as

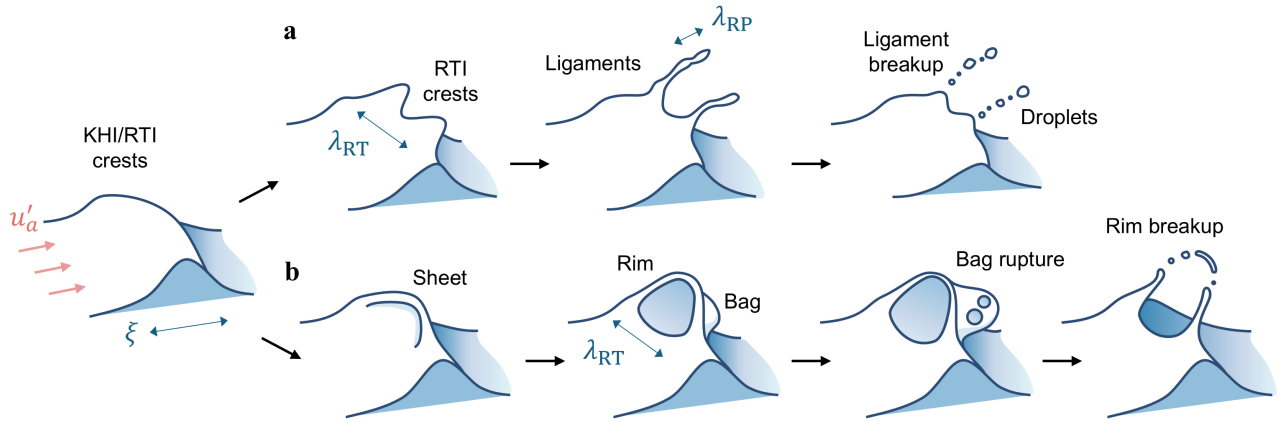


FIG. 4. Schematic illustrating sub-secondary breakup processes. The early stage KHI initiates an undulation with characteristic scale $\xi \sim \lambda_{KH}$. Beyond a particular finite amplitude, this undergoes destabilization governed by subsequent wave mechanisms, forming a non-linear wave cascade. The accelerating interface undergoes azimuthal RTI. (a) ligament mode: transverse acceleration RTI (b) bag mode: longitudinal acceleration RTI. This eventually creates terminal ligaments that generate droplets through RPI.

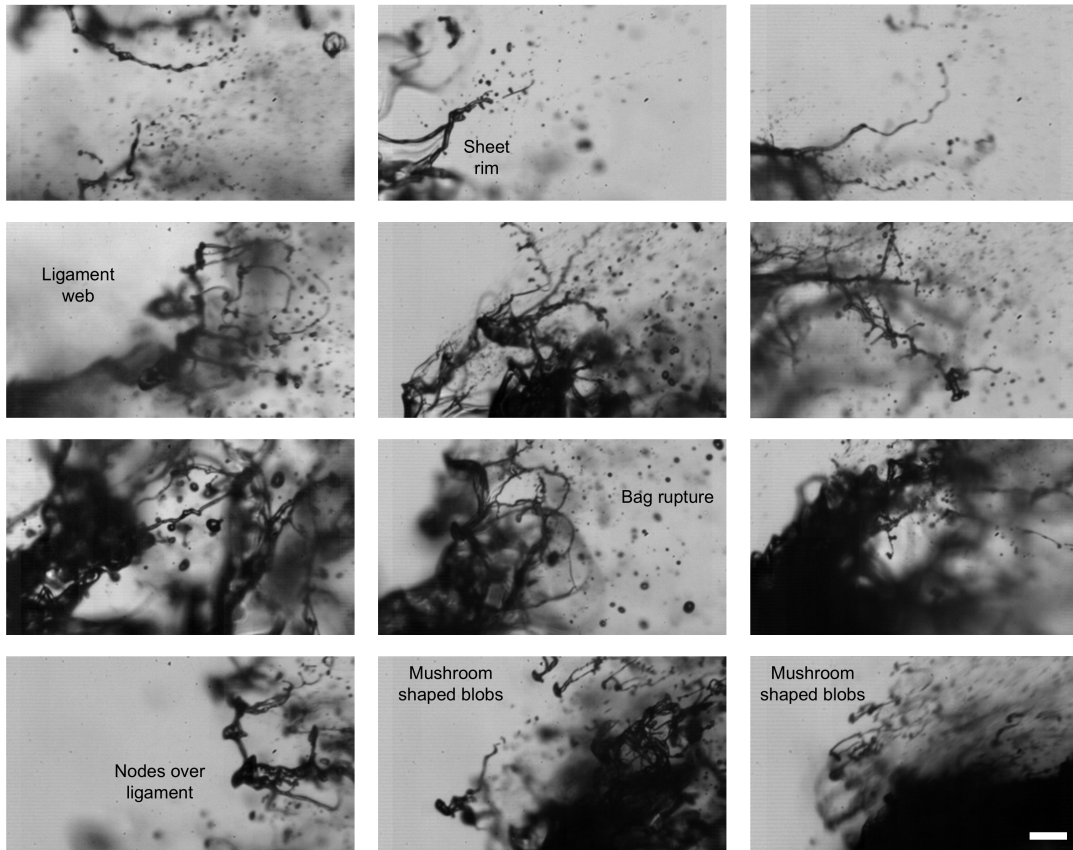


FIG. 5. Corrugated ligaments: Various ligaments observed during the aerobreakup exhibit intricate topologies and significant levels of corrugations. This catalog presents examples of ligaments that remain attached to the parent droplet or sheet or bag, as well as those that are free-standing, including mushroom-shaped blobs. Additionally, it includes intra-body ligaments and complex ligament networks that are reminiscent of a web structure. The scale bar (bottom right) represents $100\mu m$. The columns from left to right corresponds to $We \approx 900, 2000, 4000$

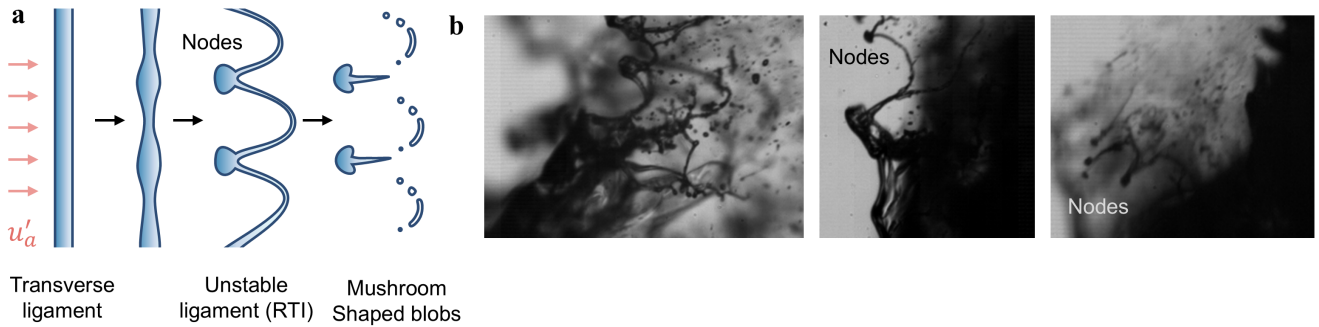


FIG. 6. RTI based Ligament breakup mechanism. (a) Schematic depicting the formation of nodes, which remain as “mushroom” blobs at the end. (b) Experimental images.

a hemispherical segment then enabled the determination of the characteristic scale which was used to determine the local effective We . These undulation can be topologically complex and shadow images present only a two-dimensional projections of the same. Hence we require high spatiotemporal measurement resolutions to capture the generated droplets to assess the equivalent volume or effective scale.

C. Ligament-mediated droplet generation

As explained earlier, the sub-secondary breakup processes ends as the undulation disintegrates into daughter droplets. However, the termination entails a final ligament-mediated mechanism as illustrated in figure 4. The corrugated ligaments portrays an inertio-capillary system with liquid inertia and surface tension forces dominating the dynamics. The ligament can be considered as a collection of a protoblobs (see figure 7) where the evolution ensure two possibilities: either the blobs separate through RPI mechanism or they coalesce into a bigger blob. Recent studies [14, 15, 27] considered these effects and emphasized the role of corrugations on this delicate balance between breakup and coalescence. These random corrugations arise from the disturbances induced at extreme flow conditions and coupled interaction between the two phases. A correlation between the ligament shape and the final daughter droplet size distribution has been established in the form of a Gamma distribution [15] or possibly a compound gamma distribution [16]

$$P_{m,n}(x = d/\langle d \rangle) = \frac{2(mn)^{(m+n)/2} x^{(m+n)/2-1}}{\Gamma(m)\Gamma(n)} \mathcal{K}_{m-n}(2\sqrt{mnx}) \quad (2)$$

where Γ is the gamma function, \mathcal{K} is the modified Bessel function of the second kind and the coefficients m and n represent ligament size distribution and corrugations. The coefficient $n = \langle d_c \rangle^2 / (\langle d_c^2 \rangle - \langle d_c \rangle^2)$ is deduced by decomposing a corrugated ligament into blobs matching local ligament diameter d_c as illustrated in figure 7. The coefficient $m = \langle l \rangle^2 / (\langle l^2 \rangle - \langle l \rangle^2)$ is deduced by taking the mean diameters $l = \langle d_c \rangle$ for various ligaments.

Considering a sample of ligaments spread across space and time with different imposed gas flow We , this corrugation factor was determined mostly to be in the range spanning $n = 3 - 8$. The values close to $n = 4$ were identified as the most frequently observed across various We flows. This corresponds to extremely corrugated ligaments and $n = 4$ is a practical limit on the coefficient considering various physical constraints [27]. Also a very low value of $m = 3$ (corresponding to the fit as illustrated in figure 9a) represent a broad ligament size (l) distribution, as observed from the experiments as well (see figure 5). This illustrates the multi-scaled nature of the atomization processes generating the intermediate features at a range of scales.

The invariance with respect to We number supports the saturation of these coefficients (especially n) to the theoretical limit. Although the sub-secondary breakup process involves the ligament production through various mechanisms, the ligaments collectively are postulated to exhibit extreme levels of corrugations, primarily due to the highly potent disruptive aerodynamic forces at extreme We . The ligaments are expected to scale down to smaller average diameters as We is increased (as observed in the experiments in figure 5), but the shape factor is already saturated and depicts values close to $n = 4$. To elucidate this hypothesis, we will consider the estimated size distribution in the subsequent sections.

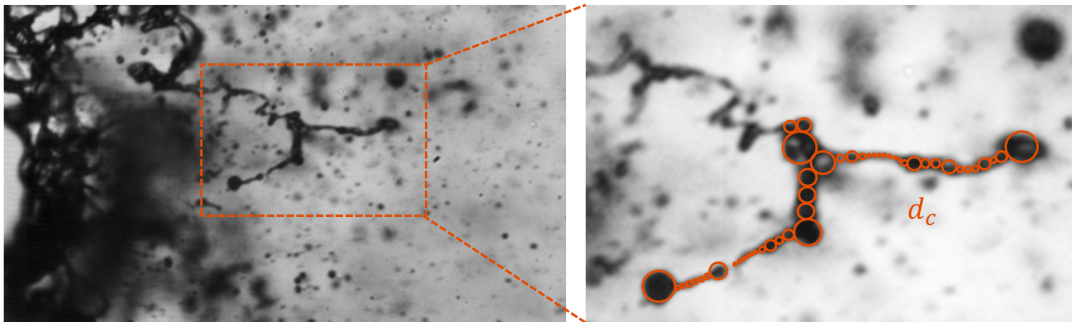


FIG. 7. A typical corrugated ligament decomposed into blobs (marked as circles) matching local ligament diameter d_c

D. Droplet size distribution

The unsteady imposition arising from this open nozzle-blast wave induced flows [18, 28, 29], the dynamics are expected to be transient. However the droplet aerobreakup intrinsically is a transient phenomenon. The recurrent wave cascade continuously strips away the liquid from the parent droplet mass and generates droplets through sub-secondary breakup processes. Hence the droplets are produced with evolving characteristics over a period of time depending on the flow around residual parent droplet. To capture this effect, droplet size measurements were performed considering the time stamp of their appearance in the measurement zone (t^*). This zone was located 30mm downstream from the parent drop for a better visibility of daughter droplets[20].

All the sampled droplets, when consolidated, gave the overall size distributions for different We flow. However, the appearance of the first and the last droplet in the zone reflects the breakup time period t_b^* , which can be subdivided into equal sub-periods. The assessment of size distributions in these periods enables the determination of transient characteristics of the system. The time scale t^* , measured from the appearance of the first droplet, is then normalized using the breakup period t_b^* such that $\tau_b = t^*/t_b^*$. The overall distributions as probability density functions (PDFs) are illustrated in figure 8a. The average droplet size decreases as We is increased. The transient PDFs are represented as a contour plot depicting a transition to observing larger droplet sizes as time progresses in figure 8b. However, if we normalize the PDFs with corresponding average droplet size d_{10}^* , we observe the different time period to follow the same underlying distribution. The same effects are visible in all We discussed in this study as illustrated in figure 8c.

For more reliable statistics with a larger sample size in each period, the breakup time is split into 3 parts, and the corresponding normalized PDFs along with global distributions are presented in in figure 9a along with the compound gamma and log-normal distribution fits. They almost overlap, especially till $d/\langle d \rangle \approx 6$. The compound gamma distribution aligns with the earlier prediction $n = 4$, deduced from the ligament-mediated mechanism. The deviation is observed consistently at the tails, which might be due to the effects like (i) The unsteady decaying airflow with lower effective We at later stages results in larger droplets being produced from the residual parent droplet and (ii) coalescence of daughter droplets. To have a better understanding, we require unsteady destabilization models and better measurement capabilities.

Since the normalized PDFs follow a common underlying distribution, the prediction of average diameter is ideally sufficient to determine actual PDFs. Sultanov and Yarin [30] assumed a chaotic isotropic deformation of the liquid mass to analytically deduce size distributions in explosive breakups, pertain high level of disruptive energy. We extend the same to present catastrophic aerobreakup. The imposed disruptive energy E induces a deformation rate of $\dot{\gamma}$ to the droplet of initial radius r_0 , such that $(1/2)\rho_l r_0^2 (\dot{\gamma} r_0)^2 \sim E$. Assuming chaotic random dispersal [30], the same deformation rate is extended to individual daughter droplets with characteristic size r_f (radius), such that the associated incremental surface energy scales as $(1/2)\rho_l r_f^2 (\dot{\gamma} r_0)^2 \sim \sigma r_f^2$. Simplifying these equations where $E \sim \rho_a u_a^2 r_0^3$ for aerobreakup, we get $(r_f/r_0) \sim We^{-1/3}$. Suspecting $d_{10} \sim d_f$, we have

$$d_{10}/d_0 \sim We^{-1/3} \quad (3)$$

This scaling relationship is validated in figure 9b. Although the observed breakup is not completely random, the hypothesis holds. Deviations from this are expected at lower We , where the breakup is evidently regular in geometry and prominently anisotropic. A similar scaling law for average droplet diameters was deduced by Kooij *et al.* [16] for flat-fan sprays, using the unstable wave-mediated sheet disintegration mechanism.

A temporal evolution of average droplet diameters d_{10}^* are also presented in figure 10a, where global averages d_{10} is used for normalization, depicting a similar trend for different We . The smaller sized droplets appear first (also see

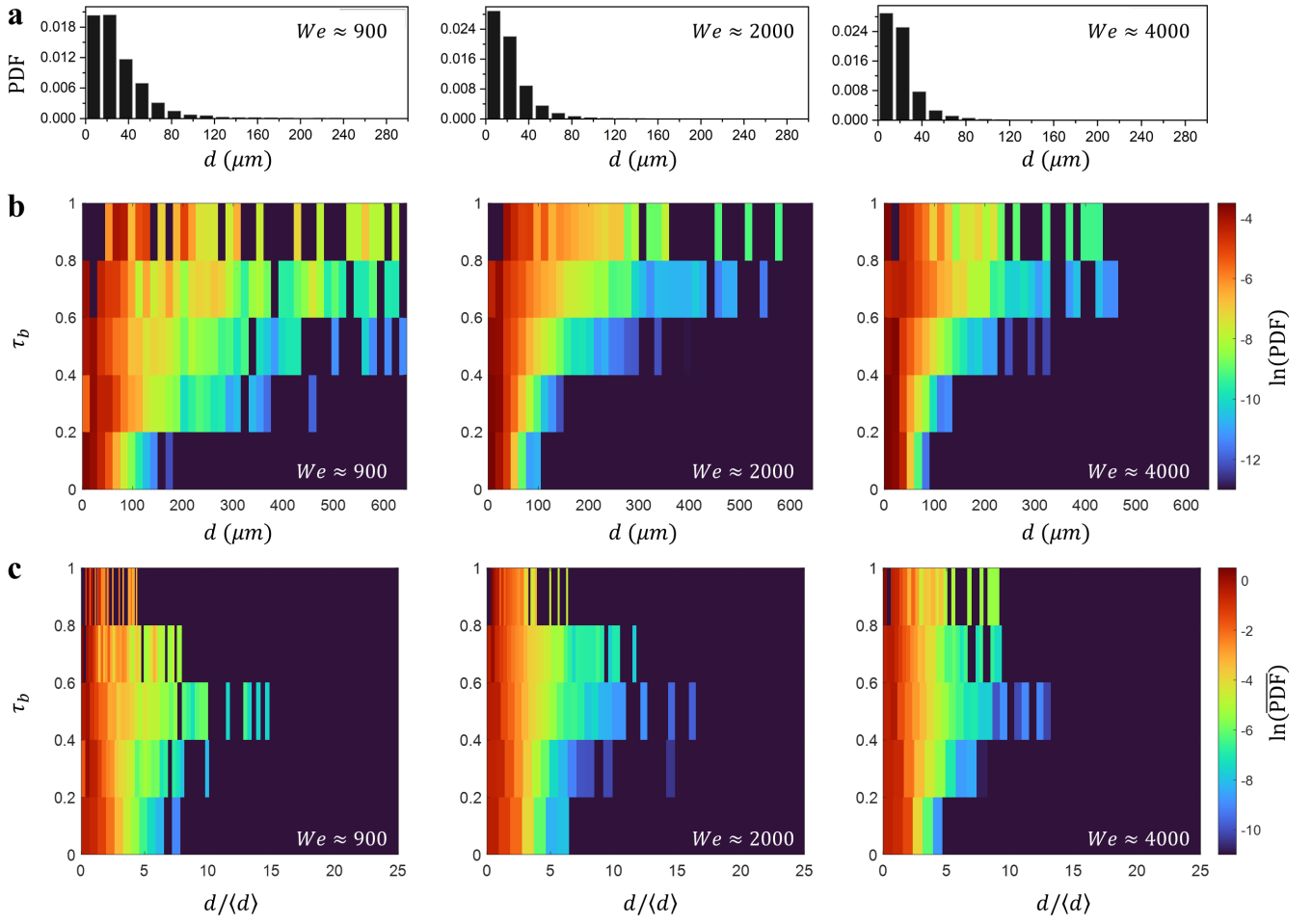


FIG. 8. (a) Overall droplet size distribution PDFs at different We . (b) Temporal evolution of PDFs represented a contour plot, where the breakup event is sub divided into 5 equal periods. (c) Temporal evolution of Normalised PDFs (using average droplet diameter $\langle d \rangle$), depicting self similar behaviour in time. Here τ_b =centre of each time period/total breakup time.

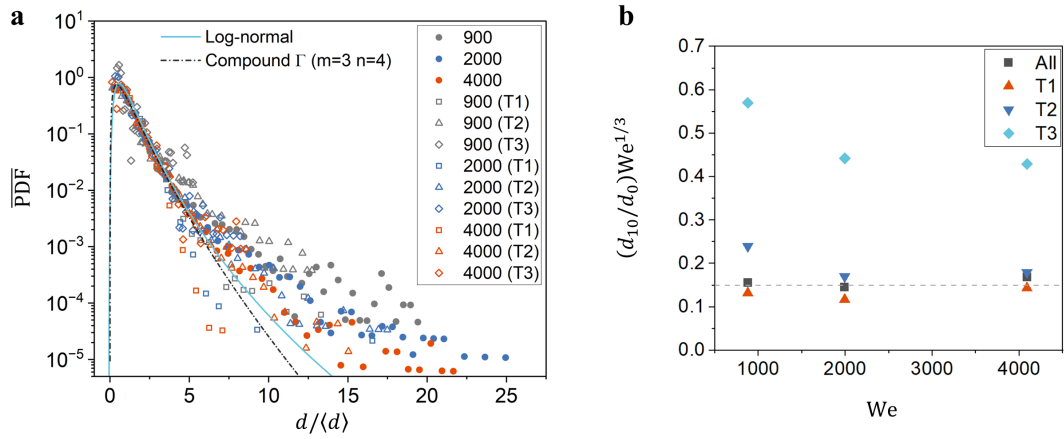


FIG. 9. Normalized PDFs depicting self-similar distributions across We and time (T1-T3 denotes equal breakup periods). (b) Invariance of We based normalized average diameters.

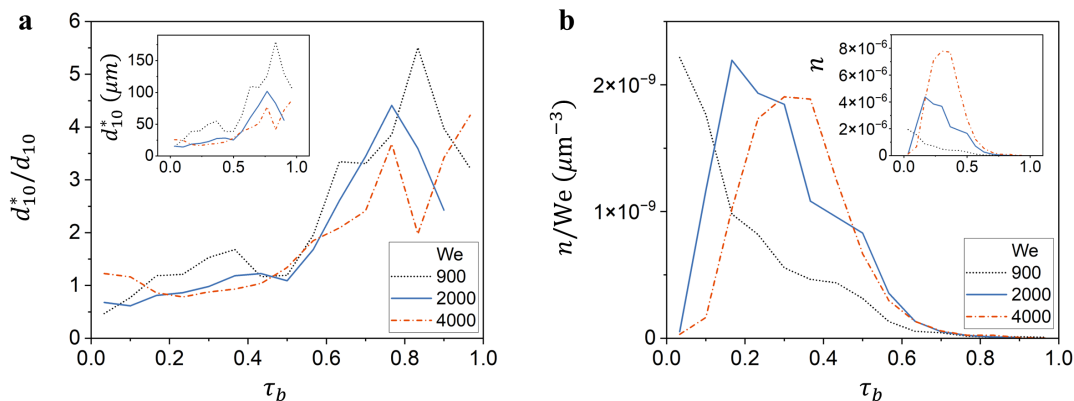


FIG. 10. Transient evolution of (a) average diameter of daughter droplets. (b) volumetric concentration of droplet frequency. They are normalized using scales based on catastrophic breakup assumption. The insets denotes non-normalized counterparts.

figure 8b) and the possible mechanisms include: (i) unsteady impulsive airflow with higher effective We generating smaller droplets during early interaction (ii) size dependent migration where smaller droplets with lower inertia reach the measurement zone first. The number of daughter droplets N can be also deduced extending earlier analysis

$$N \sim (r_0^3/r_f^3) \sim We \quad (4)$$

We consider the number of droplets produced per unit measurement volume i.e. the number concentration $n = N/V_{meas}$ for unbiased estimates of droplet count [20, 31]. Temporal evolution of the normalized version n/We is plotted in figure 10b illustrating the validity of aforementioned scales (represented by peaks). A similar trend is observed for different We , where a huge number of droplets are generated in the early stages. Culminating both the ideas (temporal evolution of d_{10}^* and n), we deduce that the droplets with smaller diameters appear first in large quantities. Since, we observe an insignificant variation in temporal evolution of d_{10}^* at all We (see inset of figure 10a), it suggests that the overall size distributions is predominantly determined by the scale associated with the maxima of n (see inset of figure 10b).

IV. CONCLUSION

In the present study, we have a closer look into the intermediate sub-scale processes that occur during the unsteady aerobreakup of a droplet in the range $We \approx 900 - 4000$ using a shock tube system. The subsequent multi-scale interfacial deformations, originating from various unstable wave mechanisms (KHI, RTI and RPI), forms a non-linear cascade. The undulations disintegrate through sub-secondary breakup processes, primarily conforming to a ligament or bag mode. The daughter droplet size distributions were estimated using a DFD technique, where the normalized distributions, at different We and time periods, followed a common fit. This compound gamma distribution parameter aligns well with the coefficient determined from terminal ligaments. This corresponds to the limit associated with most extreme corrugations physically possible. This illustrates a self-similar behavior pertaining the transient size distributions at different We , as well as the evolution of topological features at different scales (initial droplet/undulation; global/local) with an effective We bridging them.

ACKNOWLEDGMENTS

S.J.R. would like to thank the Prime Minister Research Fellowship (PMRF) for the financial support. S.B. would like to acknowledge the support from the Indian National Academy of Engineering (INAE) Chair professorship.

-
- [1] S. Sharma, N. K. Chandra, S. Basu, and A. Kumar, Advances in droplet aerobreakup, The European Physical Journal Special Topics 10.1140/epjs/s11734-022-00653-z (2022).
 [2] D. R. Guildenbecher, C. López-Rivera, and P. E. Sojka, Secondary atomization, Experiments in Fluids **46**, 371 (2009).

- [3] T. Theofanous, Aerobreakup of Newtonian and Viscoelastic Liquids, *Annual Review of Fluid Mechanics* **43**, 661 (2011).
- [4] J. Hoepffner, R. Blumenthal, and S. Zaleski, Self-Similar Wave Produced by Local Perturbation of the Kelvin-Helmholtz Shear-Layer Instability, *Physical Review Letters* **106**, 104502 (2011).
- [5] J. J. S. Jerome, S. Marty, J.-P. Matas, S. Zaleski, and J. Hoepffner, Vortices catapult droplets in atomization, *Physics of Fluids* **25**, 112109 (2013).
- [6] P. Marmottant and E. Villermaux, On spray formation, *Journal of Fluid Mechanics* **498**, 73 (2004).
- [7] A. Zandian, W. A. Sirignano, and F. Hussain, Length-scale cascade and spread rate of atomizing planar liquid jets, *International Journal of Multiphase Flow* **113**, 117 (2019).
- [8] A. Zandian, W. A. Sirignano, and F. Hussain, Planar liquid jet: Early deformation and atomization cascades, *Physics of Fluids* **29**, 062109 (2017).
- [9] A. Zandian, W. A. Sirignano, and F. Hussain, Understanding liquid-jet atomization cascades via vortex dynamics, *Journal of Fluid Mechanics* **843**, 293 (2018).
- [10] Y. Wang, K.-S. Im, and K. Fezzaa, Similarity between the Primary and Secondary Air-Assisted Liquid Jet Breakup Mechanisms, *Physical Review Letters* **100**, 154502 (2008).
- [11] P. Marmottant and E. Villermaux, Fragmentation of stretched liquid ligaments, *Physics of fluids* **16**, 2732 (2004).
- [12] A. A. Castrejón-Pita, J. Castrejón-Pita, and I. Hutchings, Breakup of liquid filaments, *Physical review letters* **108**, 074506 (2012).
- [13] T. Driessen, R. Jeurissen, H. Wijshoff, F. Toschi, and D. Lohse, Stability of viscous long liquid filaments, *Physics of fluids* **25** (2013).
- [14] S. Pal, C. Pairetti, M. Criallesi-Esposito, D. Fuster, and S. Zaleski, Statistics of drops generated from ensembles of randomly corrugated ligaments, *Physics of Fluids* **36**, 112116 (2024).
- [15] E. Villermaux, P. Marmottant, and J. Duplat, Ligament-Mediated Spray Formation, *Physical Review Letters* **92**, 074501 (2004).
- [16] S. Kooij, R. Sijs, M. M. Denn, E. Villermaux, and D. Bonn, What Determines the Drop Size in Sprays?, *Physical Review X* **8**, 031019 (2018).
- [17] S. Sharma, A. Pratap Singh, S. Srinivas Rao, A. Kumar, and S. Basu, Shock induced aerobreakup of a droplet, *Journal of Fluid Mechanics* **929**, A27 (2021).
- [18] N. K. Chandra, S. Sharma, S. Basu, and A. Kumar, Shock-induced aerobreakup of a polymeric droplet, *Journal of Fluid Mechanics* **965**, A1 (2023).
- [19] S. Sharma, N. K. Chandra, A. Kumar, and S. Basu, Shock-induced atomisation of a liquid metal droplet, *Journal of Fluid Mechanics* **972**, A7 (2023).
- [20] S. Sharma, S. J. Rao, N. K. Chandra, A. Kumar, S. Basu, and C. Tropea, Depth from defocus technique applied to unsteady shock-drop secondary atomization, *Experiments in Fluids* **64**, 65 (2023).
- [21] M. Jalaal and K. Mehravaran, Transient growth of droplet instabilities in a stream, *Physics of Fluids* **26**, 012101 (2014).
- [22] B. Dorschner, L. Biasiori-Poulanges, K. Schmidmayer, H. El-Rabii, and T. Colonius, On the formation and recurrent shedding of ligaments in droplet aerobreakup, *Journal of Fluid Mechanics* **904**, A20 (2020).
- [23] Y. Wang and L. Bourouiba, Growth and breakup of ligaments in unsteady fragmentation, *Journal of Fluid Mechanics* **910**, A39 (2021).
- [24] Y. Wang, R. Dandekar, N. Bustos, S. Poulain, and L. Bourouiba, Universal Rim Thickness in Unsteady Sheet Fragmentation, *Physical Review Letters* **120**, 204503 (2018).
- [25] I. M. Jackiw and N. Ashgriz, On aerodynamic droplet breakup, *Journal of Fluid Mechanics* **913**, A33 (2021).
- [26] N. K. Chandra, S. Sharma, S. Basu, and A. Kumar, Aerodynamic bag breakup of a polymeric droplet, *Physical Review Fluids* **9**, 113303 (2024).
- [27] B. Keshavarz, E. C. Houze, J. R. Moore, M. R. Koerner, and G. H. McKinley, Ligament Mediated Fragmentation of Viscoelastic Liquids, *Physical Review Letters* **117**, 154502 (2016).
- [28] G. Vadlamudi, A. Aravind, S. J. Rao, and S. Basu, Insights into spatio-temporal dynamics during shock-droplet flame interaction, *Journal of Fluid Mechanics* **999**, A22 (2024).
- [29] N. K. Chandra, S. Sharma, S. Basu, and A. Kumar, Elasticity affects the shock-induced aerobreakup of a polymeric droplet, *Experiments in Fluids* **65**, 75 (2024).
- [30] F. M. Sultanov and A. L. Yarin, Droplet size distribution in a percolation model for explosive liquid dispersal, *Journal of Applied Mechanics and Technical Physics* **31**, 10.1007/BF00852443 (1990).
- [31] S. J. Rao, S. Sharma, S. Basu, and C. Tropea, Depth from defocus technique: a simple calibration-free approach for dispersion size measurement, *Experiments in Fluids* **65**, 55 (2024).